Near-wall model for compressible turbulent boundary layers based on an inverse velocity transformation

By K. P. Griffin, L. Fu† AND P. Moin

1. Motivation and objectives

The largest driver of computational cost in numerical simulations of wall-bounded turbulence is typically the numerical resolution in the near-wall region. In scale-resolving simulations, e.g., wall-resolved (WR) large-eddy simulations (LESs), high spatial and temporal resolutions are required to accurately simulate the small-scale eddies near walls. Wall models, or approximate boundary conditions, can be employed to reduce the near-wall resolution requirements. The computational cost (the number of grid points multiplied by the number of time steps) for the simulation of a turbulent boundary layer scales with the Reynolds number as $Re^{2.7}$ for WRLES and $Re^{1.1}$ for wall-modeled (WM) LES (Yang & Griffin 2021). Thus, wall models lead to substantial cost savings for high-Reynolds-number applications. In simulations of the Reynolds-averaged Navier-Stokes (RANS) equations, high spatial resolution is also required to resolve the steep near-wall gradients in the mean flow. Therefore, wall models—typically referred to as wall functions in the RANS context—can also greatly accelerate numerical simulations.

In this work, a wall model for high-speed wall-bounded turbulent flows is developed in Section 2. The model is evaluated via *a-priori* testing in Section 3 and via *a-posteriori* validation in Section 4. Conclusions are drawn in Section 5. The model is suitable for deployment as a boundary condition for an outer LES or RANS solver, an inflow generation scheme or the base flow for perturbation methods, possibly with the incompressible model augmented with a wake profile for the outer layer of the boundary layer.

2. Model development

The present work focuses on the paradigm of wall stress modeling (Larsson *et al.* 2016; Bose & Park 2018). For incompressible flows, Cabot & Moin (2000) proposed using the one-dimensional simplification of the RANS streamwise momentum equation as a wall model. That is,

$$\frac{\mathrm{d}}{\mathrm{d}y}\left((\overline{\mu}+\overline{\mu}_t)\frac{\mathrm{d}\widetilde{U}}{\mathrm{d}y}\right)=0, \tag{2.1}$$

where $\overline{\mu}$, $\overline{\mu}_t$ and $\widetilde{U}$ are the dynamic viscosity, eddy viscosity and velocity profiles, respectively, and y is the wall-normal coordinate. $\overline{(\cdot)}$ denotes the Reynolds average and $\widetilde{(\cdot)}$ denotes the Favre (density-weighted) average. Throughout this work, the Favre- (density-weighted-) averaged RANS and LES equations are employed. The eddy viscosity is further

† Department of Mechanical and Aerospace Engineering and Department of Mathematics, The Hong Kong University of Science and Technology, Hong Kong

modeled as

$$\overline{\mu}_t = \kappa \overline{\rho} \sqrt{\tau_w / \overline{\rho}} \left(1 - \exp(y^+ / A^+)\right)^2, \tag{2.2}$$

where $\overline{\rho}(y)$ is the density profile. The subscript $(\cdot)_w$ denotes quantities evaluated at the wall. $\tau_w = \overline{\mu}_w (d\widetilde{U}/dy)_w$ is the wall shear stress. The superscript $(\cdot)^+$ denotes nondimensionalization by the friction velocity $u_\tau = \sqrt{\tau_w / \overline{\rho}_w}$, $\overline{\rho}_w$ and the kinematic wall viscosity $\overline{\nu}_w = \overline{\mu}_w / \overline{\rho}_w$. The von Kármán constant κ and the eddy-viscosity damping coefficient A^+ are calibrated from incompressible reference data. In this work, in order to isolate Reynolds number and compressibility effects we employ the DNS data from five incompressible turbulent channel flows (Lee & Moser 2015) with friction Reynolds numbers $Re_\tau = u_\tau \delta / \nu_w = \{182, 543, 1000, 1990, 5190\}$ (throughout this work, δ denotes the channel half height or the boundary layer thickness), and fit the least-squares optimal values of $\kappa = \{0.400, 0.408, 0.400, 0.391, 0.391\}$ and $A^+ = \{18.2, 17.4, 17.0, 16.5, 16.5\}$. Linear interpolation and constant extrapolation are used for determining the calibrated values.

For an incompressible flow, the density and dynamic viscosity are known constants. In the context of WMLES, the ODE in Eq. (2.1) is solved with two boundary conditions: (i) the no-slip wall condition and (ii) a velocity sample, which is taken from the LES at a wall-normal distance referred to as the matching location. Note that the solution procedure is iterative because the eddy viscosity depends on the wall stress (Eq. (2.2)). The computed wall stress τ_w is then applied as a momentum-flux boundary condition for the outer LES solver, which completes the two-way coupling of the wall model (inner) solution and the PDE (outer) simulation.

For compressible flow, the RANS equation for temperature can similarly be simplified to the one-dimensional form (Larsson *et al.* 2016; Bose & Park 2018), which results in a second, coupled ODE for the temperature profile, i.e.,

$$\frac{\mathrm{d}}{\mathrm{d}y}\left((\overline{\mu} + \overline{\mu}_t)\widetilde{U}\frac{\mathrm{d}\widetilde{U}}{\mathrm{d}y} + C_p\left(\frac{\overline{\mu}}{\mathrm{Pr}} + \frac{\overline{\mu}_t}{\mathrm{Pr}_t}\right)\frac{\mathrm{d}\widetilde{T}}{\mathrm{d}y}\right) = 0, \tag{2.3}$$

where $\widetilde{T}$ is the temperature profile. C_p is the specific heat capacity at constant pressure, Pr is the Prandtl number and Pr_t is the turbulent Prandtl number, which is assumed to be 0.9 (Larsson *et al.* 2016). The dependence of dynamic viscosity on temperature can be assumed to follow a power law or Sutherland's law. The ideal gas equation of state closes the system, and the thin-boundary-layer assumption implies that the pressure is constant across the inner layer.

In WMLES, the temperature ODE in Eq. (2.3) is solved with two additional boundary conditions: (i) the wall temperature and (ii) the temperature at the matching location. Note that the solution procedure is also iterative in that the temperature depends on the velocity solution. The velocity also depends on the temperature through the density and viscosity. The higher degree of nonlinearity compared to the incompressible case can prove difficult to converge in flows with strong temperature gradients (strong heat transfer), e.g., as was reported in Fu *et al.* (2021). In addition to the numerical difficulties of solving these two coupled ODEs, the accuracy of this wall model degrades substantially in flows with strong heat transfer (as will be demonstrated herein).

Improved results for high-speed wall-bounded turbulent flows over cold walls have been obtained by using the semi-local scaling in the damping function (Yang & Lv 2018; Fu *et al.* 2022); however, Iyer & Malik (2019) report that in adiabatic walls, the classical scaling (consistent with the van Driest transformation) is more accurate. This motivates

the use of a recently developed compressible velocity transformation that is accurate for both diabatic and adiabatic turbulent boundary layers (Griffin *et al.* 2021*c*).

There are three principal differences between the present model and the classical ODE-based wall model (Eqs. (2.1–2.3)): (i) rather than solving an ODE for the compressible velocity profile directly, the incompressible ODE (with constant density and viscosity) is solved and an inverse compressibility transformation (Griffin *et al.* 2021*c*) is employed; (ii) rather than employing a RANS equation for temperature and assuming a constant Pr_t, an algebraic temperature-velocity relation is adopted, thus obviating the need to solve a second ODE; and (iii) Reynolds-number-dependent coefficients are used in the incompressible ODE to improve the accuracy at low Reynolds numbers.

2.1. *Inverse compressible velocity transformation*

A compressible velocity transformation seeks to map a compressible velocity profile to an incompressible, constant-property velocity profile at an equivalent Reynolds number. In this way, a successful transformation can collapse profiles with different Mach numbers and thermal boundary conditions to a single incompressible law of the wall. Coupled with the incompressible profile implied by Eq. (2.1), an inverse velocity transformation can recover the compressible velocity profile.

The total-stress-based compressible velocity transformation of Griffin *et al.* (2021*c*) is used in this work, since it is shown to be accurate in a wide range of flows, including boundary layers with strong heat transfer. This transformation uses the viscous scaling arguments of Trettel & Larsson (2016) and Patel *et al.* (2016) in the near-wall viscous region and uses a modified version of the turbulence equilibrium arguments of Zhang *et al.* (2012) for the logarithmic region. The transformation is an algebraic function that relates the mean shear of the compressible flow, $d\widetilde{U}/dy$, to the incompressible mean shear profile, S_t^+, at the same semi-local friction Reynolds number, Re_τ^*, according to the relation

$$S_t^+ = \frac{S_{eq}^+}{1 + S_{eq}^+ - S_{TL}^+}, \tag{2.4}$$

where $S_{eq}^+ = 1/\overline{\mu}^+ d\widetilde{U}^+/dy^*$ and $S_{TL}^+ = \overline{\mu}^+ d\widetilde{U}^+/dy^+$. The superscript $(\cdot)^*$ denotes nondimensionalization by the local density $\rho(y)$, viscosity $\mu(y)$ and the semi-local friction velocity $u_{sl} = \sqrt{\tau_w/\overline{\rho}(y)}$ (Coleman *et al.* 1995; Huang *et al.* 1995). The semi-local friction Reynolds number is thus defined as $Re_\tau^* = \overline{\rho}_e u_{sl} \delta / \overline{\mu}_e$, where the subscript $(\cdot)_e$ denotes quantities evaluated at the boundary-layer edge. Note that the transformation assumes a constant stress layer in the buffer region of the boundary layer where there is a transition between the underlying viscous and equilibrium transformations. Griffin *et al.* (2021*c*) verifies that the deployment of this assumption does not significantly affect the accuracy of the transformation in channel flows, pipe flows and zero-pressure-gradient boundary layers, and Bai *et al.* (2022) verifies the same for boundary layers with moderate pressure gradients.

The inverse velocity transformation is readily obtained by algebraically rearranging the transformation to find

$$\frac{\mathrm{d}\widetilde{U}^+}{\mathrm{d}y^*} = \left(\frac{1}{\overline{\mu}^+ S_t^+} - \frac{1}{\overline{\mu}^+} + \sqrt{\overline{\rho}^+} \left(1 + \frac{1}{2\overline{\rho}^+} \frac{\mathrm{d}\overline{\rho}^+}{\mathrm{d}y^+} y^+ - \frac{1}{\overline{\mu}^+} \frac{\mathrm{d}\overline{\mu}^+}{\mathrm{d}y^+} y^+ \right) \right)^{-1}. \tag{2.5}$$

The incompressible mean shear S_t^+ is available algebraically from the constant property version of Eq. (2.1), i.e., $\overline{\rho} = \overline{\rho}_w$ and $\overline{\mu} = \overline{\mu}_w$. The incompressible model constants κ and B are determined using the aforementioned calibration, but Re_τ^* is used in place of

Re_τ since the former is invariant under the velocity transformation. Integrating Eq. (2.5) with variable properties yields the targeted compressible velocity profile; the properties are functions of temperature, which will be discussed next.

2.2. *Algebraic temperature-velocity relation*

The analogy between the conservation equations for momentum and energy has led to the derivation of several algebraic relations between temperature and velocity. The most widely validated such relation was proposed by Duan & Martín (2011). Walz's equation (also known as the modified Crocco-Busemann relation) leverages the analogy between the conservation equations for momentum and energy to arrive at an algebraic relation between mean temperature and velocity. This relation accounts for non-unity Pr effects via a recovery factor, which is taken as $r = (\mathrm{Pr})^{1/3}$. While this relation is accurate in high-speed adiabatic boundary layers, Duan & Martín (2011) observed that the accuracy degrades significantly in boundary layers with wall heat transfer and proposed a semi-empirical correction to the relation. This was subsequently recast in terms of a generalized Reynolds analogy (Zhang *et al.* 2014), thereby introducing the Reynolds analogy factor, s, which they choose as $s = 1.14$ following convention. The resulting temperature-velocity relation is given as

$$\widetilde{T} = \widetilde{T}_w + s\,\mathrm{Pr}(\widetilde{T}_r - \widetilde{T}_w)\frac{\widetilde{U}}{\widetilde{U}_e}\left(1 - \frac{\widetilde{U}}{\widetilde{U}_e}\right) + \left(\frac{\widetilde{U}}{\widetilde{U}_e}\right)^2\left(\widetilde{T}_e - \widetilde{T}_w\right), \tag{2.6}$$

where the subscript $(\cdot)_e$ denotes quantities at the boundary-layer edge, the recovery temperature $\widetilde{T}_r = \widetilde{T}_e + r\widetilde{U}_e^2/(2C_p)$. This relation has been validated across a wide range of channel flows, pipe flows and boundary layers with and without heat transfer (Zhang *et al.* 2014, 2018; Modesti & Pirozzoli 2019; Volpiani *et al.* 2020; Fu *et al.* 2021). Specifically, this relation is derived by Zhang *et al.* (2014) through defining the generalized recovery temperature $\widetilde{T}_{r_g} = \widetilde{T} + r_g\widetilde{U}^2/(2C_p)$. Then, it is assumed that $\widetilde{T}_{r_g} = \widetilde{T}_w + U_s\widetilde{U}/C_p$, where U_s is a constant velocity scale. Equivalently, the assumption can be reinterpreted that $\widetilde{T}$ can be approximately represented as a second-order Taylor expansion in terms of powers of $\widetilde{U}$, i.e.,

$$\widetilde{T} = b_0 + b_1\widetilde{U} + b_2\widetilde{U}^2/2, \tag{2.7}$$

where the no-slip condition implies $b_0 = \widetilde{T}_w$, $b_1 = (\mathrm{d}\widetilde{T}/\mathrm{d}\widetilde{U})|_w$. The algebraic relation of Zhang *et al.* (2014) can be recovered if b_2 is specified by evaluating the expression at the boundary-layer edge $\widetilde{T}_e = \widetilde{T}|_{\widetilde{U}_e}$ and b_1 is determined using the Reynolds analogy. However, in this work, we use the matching data [denoted with subscript $(\cdot)_m$] $\widetilde{T}_m = \widetilde{T}|_{\widetilde{U}_m}$ to set b_2, such that the exact value at the matching location can be enforced. The final temperature-velocity relation is

$$\widetilde{T} = \widetilde{T}_w + s\,\mathrm{Pr}(\widetilde{T}_r - \widetilde{T}_w)\frac{\widetilde{U}}{\widetilde{U}_e}\left(1 - \frac{\widetilde{U}}{\widetilde{U}_m}\right) + \left(\frac{\widetilde{U}}{\widetilde{U}_m}\right)^2\left(\widetilde{T}_m - \widetilde{T}_w\right). \tag{2.8}$$

Note that one consequence of this relation is that the wall heat flux and wall shear stress are algebraically linked by the Reynolds analogy factor, where the heat flux is defined as $q_w = s\tau_w C_p(\widetilde{T}_w - \widetilde{T}_r)/\widetilde{U}_e$.

2.3. *Implementation details*

Like the classical model (Eqs. (2.1–2.3)), the present model requires a matching temperature, velocity and density, an equation of state (the ideal gas law is used in this work, and the thin-boundary-layer assumption implies the pressure is constant), and a viscosity law (either a power law or Sutherland's law, depending on the relevant reference data). In addition, the present model requires as input the velocity and temperature at the boundary-layer edge [computed using the method of Griffin *et al.* (2021*a*)] for deploying the algebraic temperature-velocity relation. To solve the nonlinear system, the following approach is used. The incompressible ODE (Eq. (2.1)) with constant properties (with κ and A^+ determined by Re_τ^*) is substituted into the inverse velocity transformation (Eq. (2.5)). This equation (initial value problem with an initial guess for the wall shear stress) is solved via the shooting method, where, at each integration step, a sub-iteration determines the velocity increment that is consistent with the temperature-velocity relation (Eq. (2.8)) and the resulting density and viscosity at that location. A similar procedure was used by Griffin *et al.* (2021*b*).

3. *A-priori* results

The present and classical wall models are first evaluated via *a-priori* analysis. That is, the matching data is taken from DNS at a wall-normal distance of $y_m = 0.3\delta$. The wall model estimates the velocity and temperature profiles as well as the wall shear stress and wall heat flux. The predicted velocity and temperature profiles are shown in Figure 1 for two flows. Figure 1(a,b) shows the results from a supersonic channel flow with a bulk Mach number $M_b = U_b/\sqrt{(\gamma R \widetilde{T}_w)} = 1.7$ and a bulk Reynolds number $Re_b = \rho_b U_b \delta/\overline{\mu}_w = 10000$, where the bulk density is defined as $\rho_b = \int_0^\delta \overline{\rho} dy/\delta$ and the bulk velocity is defined as $U_b = \int_0^\delta \widetilde{U} dy/\delta$, with DNS data from Trettel & Larsson (2016). Figure 1(c,d) shows the results for a hypersonic diabatic boundary layer with an edge Mach number of 5.0 and a semi-local friction Reynolds number of 2300, with DNS data from Volpiani *et al.* (2020). The profiles predicted by the present model agree with the DNS profiles significantly better than the classical model. Note that the velocities are nondimensionalized by the predicted friction velocity, so the obtained profiles do not necessarily pass through the matching data if the predicted wall stress is inaccurate.

Next, the model performance is evaluated with a wide range of DNS data from 48 different simulations. The errors in the modeled wall stress and heat flux predictions are reported for each case with $y_m = 0.3\delta$. The relative error in the wall stress prediction ϵ_{τ_w} is defined as

$$\epsilon_{\tau_w} = \frac{\tau_{w,\text{model}} - \tau_{w,\text{DNS}}}{\tau_{w,\text{DNS}}} \times 100\%. \tag{3.1}$$

The nondimensional wall heat flux is defined as $B_q = q_w/(C_p \widetilde{T}_w \overline{\rho}_w u_\tau)$, and the relative error in the wall heat flux is defined as

$$\epsilon_{q_w} = \frac{q_{w,\text{model}} - q_{w,\text{DNS}}}{q_{w,\text{DNS}}} \times 100\%. \tag{3.2}$$

ϵ_{q_w} is not reported for adiabatic boundary layer data because it is undefined, and both models predict negligible heat transfer for these data. The data considered include the compressible channel flow simulations of Modesti & Pirozzoli (2016), Trettel & Larsson (2016) and Yao & Hussain (2020); the pipe flow simulations of Modesti & Pirozzoli (2019);

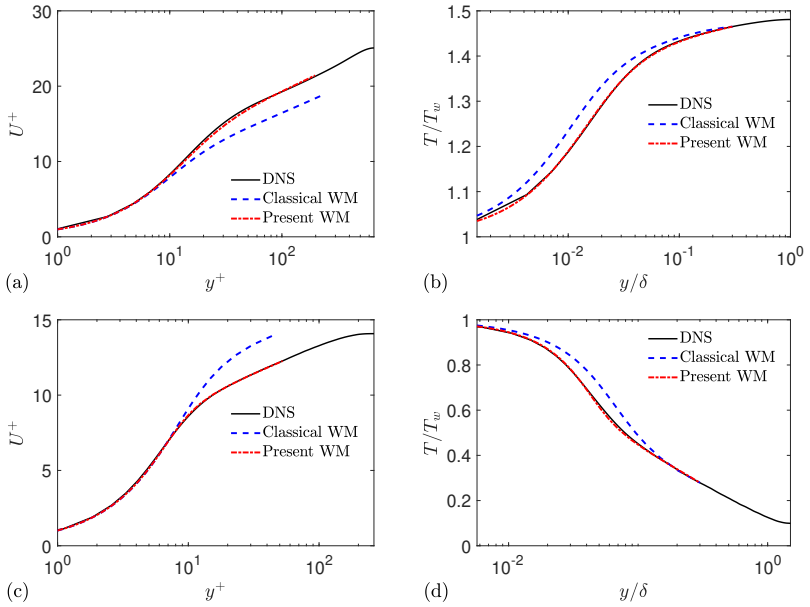

FIGURE 1. *A-priori* wall-modeled profiles of (a,c) velocity and (b,d) temperature are plotted versus the wall-normal coordinate. Panels (a) and (b) are for a supersonic channel flow; panels (c) and (d) are for a hypersonic diabatic boundary layer.

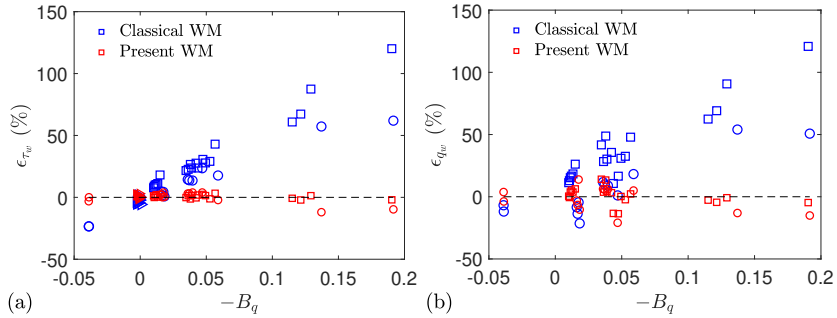

FIGURE 2. *A-priori* modeling errors of (a) the wall shear stress τ_w and (b) the wall heat flux q_w versus the heat transfer coefficient B_q. The model matching data is taken from DNSs of various channel and pipe flows (squares), nearly adiabatic boundary layers (triangles), and diabatic boundary layers (circles).

the adiabatic supersonic and hypersonic boundary layers of Pirozzoli & Bernardini (2011), Zhang *et al.* (2018), Volpiani *et al.* (2018) and Volpiani *et al.* (2020); and the diabatic supersonic and hypersonic boundary layers of Zhang *et al.* (2018), Volpiani *et al.* (2018, 2020) and Fu *et al.* (2019). The cases have edge Mach numbers in the range of 0.77–11 and semi-local friction Reynolds numbers in the range of 170–5700. Only the cases with $Re_\tau^* > 150$ are analyzed, because lower Reynolds numbers can exhibit strong Reynolds number effects (Modesti & Pirozzoli 2016) and are not the target of this study. The error measures are shown in Figure 2. The present model generates significantly less modeling error than the classical model, with the greatest error reduction observed when the nondimensional heat transfer is the highest.

M_b	0.6998	0.6999	1.698	1.699	1.699	2.994	2.996	2.997	3.993
Re_b	7498	11750	4495	9993	15490	7486	14980	23980	9979
Re_τ	436.6	650.9	318.6	661.6	963.6	636.4	1208	1842	1010.
Re_τ^*	395.7	590.0	194.8	405.4	590.8	204.0	387.7	589.7	201.3
$-100B_q$	1.061	1.009	5.668	5.273	4.942	12.92	12.15	11.50	19.04

TABLE 1. Nondimensional flow parameters for the nine compressible turbulent channel flow cases considered for *a-posteriori* testing within the WMLES framework.

4. *A-posteriori* WMLES results

In this section, several WMLES simulations are conducted using charLES, a high-fidelity compressible finite-volume code (Brès *et al.* 2018). The numerical method consists of a low-dissipation, approximately entropy-preserving scheme that utilizes artificial bulk viscosity to capture the solution discontinuities. Additional details about the solver and a summary of validation campaigns are available in Fu *et al.* (2021, 2022).

The WMLESs conducted herein are compressible turbulent channel flows driven with uniform volumetric momentum and energy source terms to achieve the same bulk Mach number and bulk Reynolds number conditions of the DNS simulations of Trettel & Larsson (2016), as summarized in Table 1. The cases are run on a domain of size $(\pi \times 2 \times \pi\sqrt{3}/4)\delta$ with periodic boundary conditions in the streamwise (first) and spanwise (third) dimensions. The mean profiles and fluxes were insensitive to doubling of the streamwise and spanwise domain sizes. Consistent with the DNS simulations, the viscosity is described by $\mu/\mu_{ref} = (T/T_{ref})^{0.75}$ and $Pr = 0.7$. All cases are initialized from a uniform solution with the target bulk Mach number and Reynolds number, and zero velocity in the wall-normal and spanwise directions. The simulations are allowed to transition from laminar to turbulent states naturally and are run for ∼500 eddy turnover times δ/u_τ. To challenge the wall model and isolate the effect of near-wall numerical errors (Kawai & Larsson 2012), the wall model matching location is placed at $y_m = 0.3\delta$ and a coarse grid of 12 points per half channel height is used for all simulations unless otherwise indicated.

The velocity and temperature profiles from WMLES are shown in Figure 3. The highest Reynolds number case simulated ($M_b = 2.997$ and $Re_\tau = 1842$) is shown in Figure 3(a,b) and the highest Mach number case ($M_b = 3.993$ and $Re_\tau = 1010$) is shown in Figure 3(c,d). In both cases, the present model is significantly more accurate than the classical model for the prediction of velocity and temperature with respect to the reference DNS solutions. For these cases and the others listed in Table 1, the errors in the predictions of the wall shear stress and the wall heat flux are shown in Figure 4. The wall model is based on the inversion of the total-stress-based velocity transformation (Griffin *et al.* 2021*c*) and that was observed to have the greatest improvement over classical approaches in cases with strong heat transfer. This explains why the errors from the classical wall model grow significantly with the nondimensional heat transfer, but the errors from the present model are rather small and do not vary with heat flux.

5. Conclusions

In this work, a wall model is proposed for turbulent wall-bounded flows with heat transfer. The model uses an established ODE description of incompressible flow, transforms that equation to account for compressibility effects and is closed with an algebraic

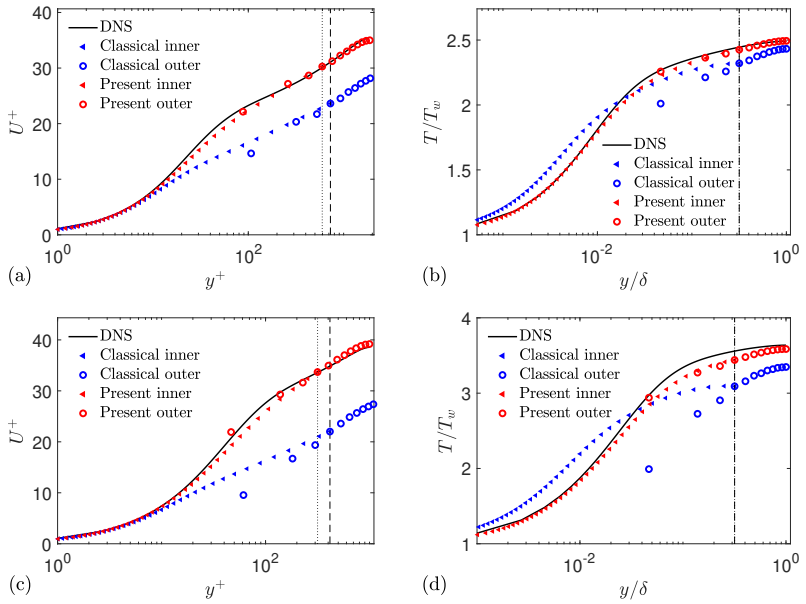

FIGURE 3. (a,c) Velocity and (b,d) temperature profiles from WMLES with the classical (red) and present (blue) wall models. A channel flow with $M_b = 2.997$ and $Re_\tau = 1842$ is shown in panels (a) and (b), and one with $M_b = 3.993$ and $Re_\tau = 1010$ is shown in panels (c) and (d). Within the WMLES framework, the outer solutions are computed by the LES PDE solver, while the inner solutions are computed by the two wall models. These solutions coincide at the LES matching point nearest to $y_m = 0.3\delta$, which is indicated with the dashed and dotted lines for the classical and present models, respectively.

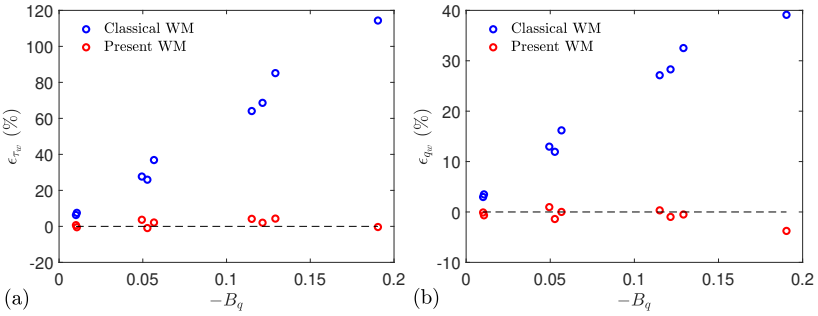

FIGURE 4. WMLES *a-posteriori* modeling errors for (a) the wall shear stress τ_w and (b) the wall heat flux q_w versus the nondimensional heat flux B_q. WMLES is conducted using the classical (red) and present (blue) wall models for turbulent channel flows at the nine operating conditions listed in Table 1.

temperature-velocity relation. The resulting model can accurately estimate the near-wall profiles of temperature and velocity when the matching location is in the inner layer. This model is suitable for deployment as a boundary condition for an outer LES or RANS solver, an inflow generation scheme, or the base flow for perturbation methods, possibly with the incompressible model augmented with a wake profile for the outer layer of the boundary layer.

The model is first tested *a-priori* to verify that it can recover the boundary layer ve-

locity and temperature data when provided with matching data from DNS. Numerical results reveal that the model accurately recovers the targeted profiles well, and the predicted wall stress and heat flux are within a few percent of their expected values for a wide database of DNS data for high-Mach-number turbulent channel flows, pipe flows and boundary layers (48 cases with edge Mach numbers in the range of 0.77–11 and semi-local friction Reynolds numbers in the range of 170–5700). The model is also tested *a-posteriori* as a boundary condition for WMLES in turbulent channel flows with bulk Mach numbers $M_b = 0.7$–4.0 and $Re_\tau = 320$–1800. The proposed model is substantially more accurate than the classical ODE-based near-wall model, especially in flows with strong wall heating, due to the fact that velocity transformation (Griffin *et al.* 2021*c*) employed accurately accounts for the compressibility effects.

Acknowledgments

K.G acknowledges support from the National Defense Science and Engineering Graduate Fellowship, the Stanford Graduate Fellowship, and the Stanford Lieberman Fellowship. L.F acknowledges funding from the Guangdong Basic and Applied Basic Research Foundation (No. 2022A1515011779) and from the Research Grants Council (RGC) of the Government of Hong Kong Special Administrative Region (HKSAR) with RGC/ECS Project (No. 26200222). P.M acknowledges support from NASA grant (No. NNX15AU93A). Declaration of Interests. The authors report no conflict of interest. The authors gratefully acknowledge helpful comments from Sanjeeb T. Bose.

REFERENCES

Bai, T., Griffin, K. P. & Fu, L. 2022 Compressible velocity transformations for various noncanonical wall-bounded turbulent flows. *AIAA J.* **60**, 4325–4337.

Bose, S. T. & Park, G. I. 2018 Wall-modeled large-eddy simulation for complex turbulent flows. *Annu. Rev. Fluid Mech.* **50**, 535–561.

Brès, G. A., Bose, S. T., Emory, M., Ham, F. E., Schmidt, O. T., Rigas, G. & Colonius, T. 2018 Large-eddy simulations of co-annular turbulent jet using a voronoi-based mesh generation framework. *AIAA Paper* 3302.

Cabot, W. H. & Moin, P. 2000 Approximate wall boundary conditions in the large-eddy simulation of high Reynolds number flow. *Flow Turbul. Combust.* **63**, 269–291.

Choi, H. & Moin, P. 2012 Grid-point requirements for large eddy simulation: Chapman's estimates revisited. *Phys. Fluids* **24**, 011702.

Coleman, G. N., Kim, J. & Moser, R. D. 1995 A numerical study of turbulent supersonic isothermal-wall channel flow. *J. Fluid Mech.* **305**, 159–183.

Duan, L. & Martín, M. P. 2011 Direct numerical simulation of hypersonic turbulent boundary layers. Part 4. Effect of high enthalpy. *J. Fluid Mech.* **684**, 25–59.

Fu, L., Bose, S. & Moin, P. 2022 Prediction of aerothermal characteristics of a generic hypersonic inlet flow. *Theor. Comput. Fluid Dyn.* **36**, 345–368.

Fu, L., Karp, M., Bose, S. T., Moin, P. & Urzay, J. 2019 Turbulence statistics in a highly supersonic boundary layer downstream of an incident shock wave. *Annual Research Briefs*, Center for Turbulence Research, Stanford University, pp. 41–54.

Fu, L., Karp, M., Bose, S. T., Moin, P. & Urzay, J. 2021 Shock-induced heating and transition to turbulence in a hypersonic boundary layer. *J. Fluid Mech.* **909**, A8.

Griffin, K. P., Fu, L. & Moin, P. 2021*a* General method for determining the boundary layer thickness in nonequilibrium flows. *Phys. Rev. Fluids* **6**, 024608.

Griffin, K. P., Fu, L. & Moin, P. 2021*b* The effect of compressibility on grid-point and time-step requirements for simulations of wall-bounded turbulent flows. *Annual Research Briefs*, Center for Turbulence Research, Stanford University, pp. 109–117.

Griffin, K. P., Fu, L. & Moin, P. 2021*c* Velocity transformation for compressible wall-bounded turbulent flows with and without heat transfer. *Proc. Natl. Acad. Sci.* **118**, e2111144118.

Huang, P. G., Coleman, G. N. & Bradshaw, P. 1995 Compressible turbulent channel flows: DNS results and modelling. *J. Fluid Mech.* **305**, 185–218.

Iyer, P. S. & Malik, M. R. 2019 Analysis of the equilibrium wall model for high-speed turbulent flows. *Phys. Rev. Fluids* **4**, 074604.

Kawai, S. & Larsson, J. 2012 Wall-modeling in large eddy simulation: Length scales, grid resolution, and accuracy. *Phys. Fluids* **24**, 015105.

Larsson, J., Kawai, S., Bodart, J. & Bermejo-Moreno, I. 2016 Large eddy simulation with modeled wall-stress: recent progress and future directions. *Mech. Eng. Rev.* **3**, 15-00418.

Lee, M. & Moser, R. D. 2015 Direct numerical simulation of turbulent channel flow up to $Re_\tau = 5200$. *J. Fluid Mech.* **774**, 395–415.

Modesti, D. & Pirozzoli, S. 2016 Reynolds and Mach number effects in compressible turbulent channel flow. *Int. J. Heat Fluid Flow* **59**, 33–49.

Modesti, D. & Pirozzoli, S. 2019 Direct numerical simulation of supersonic pipe flow at moderate Reynolds number. *Int. J. Heat Fluid Flow* **76**, 100–112.

Patel, A., Boersma, B. J. & Pecnik, R. 2016 The influence of near-wall density and viscosity gradients on turbulence in channel flows. *J. Fluid Mech.* **809**, 793–820.

Pirozzoli, S. & Bernardini, M. 2011 Turbulence in supersonic boundary layers at moderate Reynolds number. *J. Fluid Mech.* **688**, 120–168.

Trettel, A. & Larsson, J. 2016 Mean velocity scaling for compressible wall turbulence with heat transfer. *Phys. Fluids* **28**, 026102.

Volpiani, P. S., Bernardini, M. & Larsson, J. 2018 Effects of a nonadiabatic wall on supersonic shock/boundary-layer interactions. *Phys. Rev. Fluids* **3**, 083401.

Volpiani, P. S., Bernardini, M. & Larsson, J. 2020 Effects of a nonadiabatic wall on hypersonic shock/boundary-layer interactions. *Phys. Rev. Fluids* **5**, 014602.

Yang, X. I. A. & Griffin, K. P. 2021 Grid-point and time-step requirements for direct numerical simulation and large-eddy simulation. *Phys. Fluids* **33**, 015108.

Yang, X. I. A. & Lv, Y. 2018 A semi-locally scaled eddy viscosity formulation for LES wall models and flows at high speeds. *Theor. Comput. Fluid Dyn.* **32** (5), 617–627.

Yao, J. & Hussain, F. 2020 Turbulence statistics and coherent structures in compressible channel flow. *Phys. Rev. Fluids* **5**, 084603.

Zhang, C., Duan, L. & Choudhari, M. M. 2018 Direct numerical simulation database for supersonic and hypersonic turbulent boundary layers. *AIAA J.* **56**, 4297–4311.

Zhang, Y. S., Bi, W. T., Hussain, F., Li, X. L. & She, Z. S. 2012 Mach-number-invariant mean-velocity profile of compressible turbulent boundary layers. *Phys. Rev. Lett.* **109**, 054502.

Zhang, Y. S., Bi, W. T., Hussain, F. & She, Z.-S. 2014 A generalized Reynolds analogy for compressible wall-bounded turbulent flows. *J. Fluid Mech.* **739**, 392–420.